Hindawi
Shock and Vibration
Volume 2020, Article ID 9834324, 13 pages
https://doi.org/10.1155/2020/9834324

Research Article

Radial Vibration Characteristics of Piezoelectric Ceramic Composite Ultrasonic Transducer

Chundong Yao, Chao Zhang, Jiani Zhang, and Yang Zhang

School of Mechanical Engineering, Yanshan University, Qinhuangdao, China

Correspondence should be addressed to Chao Zhang; 18848973272@163.com

Received 15 February 2020; Revised 14 May 2020; Accepted 23 June 2020; Published 16 July 2020

Academic Editor: Roberto Palma

Different from the existing equivalent circuit analysis method of the transducer, based on the vibration theory of the mechanical system and combined with the constitutive equation, this paper analyzes the radial vibration characteristics of the transducer. The piezoelectric ceramic composite ultrasonic transducer is simplified as a mechanical model of a composite thick wall tube composed of a piezoelectric ceramic tube and a metal prestressed tube. The mathematical model of radial vibration of the transducer is established, which consists of the wave equation of radial coupling vibration of the piezoelectric ceramic tube and the metal prestressed tube, the continuity conditions, and the boundary conditions of radial vibration of composite thick wall tube. The characteristic equation and the mode function of radial vibration are derived. The calculated results of natural frequency are in good agreement with the existing experimental results. Based on the analytical method and the difference method, the numerical simulation models of radial vibration are established, and the amplitude-frequency characteristic curves and the displacement responses are given. The simulation results show that the amplitude-frequency characteristic curves and the displacement responses of the two methods are the same, which verifies the correctness of simulation results. Through the simulation analysis, the influence rule of the transducer's structure sizes on its radial vibration natural frequency is given: when the thickness of the metal prestressed tube and the piezoelectric ceramic tube are constant, the natural frequency decreases with the increase of the inner diameter of the piezoelectric ceramic tube; when the outer diameter of the metal prestressed tube and the inner diameter of the piezoelectric ceramic tube are constant, the natural frequency decreases with the increase of the thickness-to-wall ratio. The calculation method of natural frequency based on elastic vibration theory is clear in concept and simple in calculation, and the simulation models can analyze the mechanical vibration of the transducer.

1. Introduction

Ultrasonic transducer is one of the most important parts of an ultrasonic vibration system. Since the Curie brothers discovered the piezoelectric effect in 1880 and the French physicist Langevin invented piezoelectric transducers in 1916 [1, 2], piezoelectric ceramic transducer has gradually become the most widely used type of transducer. Piezoelectric ceramic composite ultrasonic transducer has been the research focus of experts and scholars in recent years. Because of its outstanding advantages of stable performance, large acoustic radiation area, high radiation efficiency, uniform directivity, high sensitivity, and so on [3], it is widely used in underwater acoustic receiving or transmitting [4–6].

Piezoelectric ceramic composite ultrasonic transducer is composed of a piezoelectric ceramic tube and a metal prestressed tube along radial direction, and the assembling method is the temperature difference method [7, 8]. In order to obtain the optimal working state of the transducer, the operating frequency of the transducer needs to be its natural frequency [9, 10]. Therefore, it is extremely important to study the radial vibration characteristics of the transducer.

In recent years, many scholars have done a lot of researches on the radial vibration characteristics of this kind of transducers. Based on the theory of elasticity, the vibration and stress in the length and radius direction of the thin walled piezoelectric ceramic short tube are ignored; references [11, 12] discussed the natural frequency of transducer through its equivalent circuit. For a transducer whose length

is much larger than its radial dimension, reference [13] regarded it as the plane strain problem in mechanics approximately, its pure radial vibration is analyzed, and its equivalent circuit and frequency equation are obtained. According to the principle of electromechanical analogy, reference [14] studied a kind of composite piezoelectricity ultrasonic transducer and obtained the equivalent circuit and frequency equation of the system. Reference [15] proposed a tangential polarized composite cylindrical transducer, which is connected by a tangential polarized piezoelectric tube and an outer metal circular tube, and its natural frequency is analyzed. Reference [16] developed a transducer composed of two radially reinforced composite vibrators, derived the electromechanical equivalent circuit, and obtained the input impedance of the transducer. Although the structures of those transducers studied in the above literatures are different, the essence is the analysis of the coupling vibration between piezoelectric ceramic ring (tube) and metal circular ring (tube). The main research method is to derive the equivalent circuit of transducer combined in the constitutive equation, so as to analyze the natural frequency and performance parameters of the transducer in the resonance state. The calculation process of the above method is complicated, which can only describe the performance parameters of the transducer in the resonance state, not the mechanical vibration. However, dynamic performance is closely related to its sensitivity analysis and structural optimization, which causes certain limitations to the equivalent circuit method.

The natural frequency is determined by the structure, the boundary conditions, and the continuous conditions of the vibration system [17]. Based on the vibration theory of the mechanical system and combined with the constitutive equation, the natural frequency and displacement response are obtained. So far, there is no relevant report. Compared with the equivalent circuit method, the calculation process of this method is simpler, and it can describe the mechanical vibration of transducers, which also provides theoretical support for the sensitivity analysis and optimal design of transducers. This paper studies this method. The piezoelectric ceramic composite ultrasonic transducer is simplified as a mechanical model of a composite thick wall tube composed of a piezoelectric ceramic tube and a metal prestressed tube. The mathematical model of radial vibration of the transducer is established, which consists of the wave equation of radial coupling vibration of the piezoelectric ceramic tube and the metal prestressed tube, the continuity conditions, and the boundary conditions of radial vibration of composite thick wall tube. The characteristic equation and mode function of the radial vibration of the transducer are established. Based on the analytical method and the difference method, the numerical simulation models of the radial vibration of the transducer are established, and the amplitude-frequency characteristic curves and the displacement responses of the radial vibration are given. The relationship between the natural frequency of radial vibration and structure sizes was discussed. This paper will provide some guidance for the design and application of the transducer.

2. Mechanical and Mathematical Model of Radial Vibration of the Transducer

2.1. Mechanical Model. To facilitate research, the following assumptions are made: (1) the axial dimension of the transducer largely outweigh its radial dimension. According to the problem of plane strain in elastic mechanics [18], its axial vibration is ignored, and it is analyzed as a pure radial vibration; (2) the influence of tangential stress is ignored; (3) the influence of the shrink range between the piezoelectric ceramic tube and the metal prestressed tube is ignored.

Figure 1 shows a schematic diagram of a piezoelectric ceramic composite ultrasonic transducer. It is composed of a piezoelectric ceramic tube and a metal prestressed tube with a negative tolerance by the temperature difference method. A radial excitation voltage is applied to the piezoelectric ceramic tube, which causes the metal prestressed tube to produce radial mechanical vibration by the inverse piezoelectric effect, so that the transducer can produce radial radiation of sound.

Figure 2 shows the mechanical model of the transducer. r_a, r_b are the inside and the outside diameters of the piezoelectric ceramic tube. r_b, r_c are the inside and the outside diameters of the metal prestressed tube. P_e is the environmental load.

2.1.1. Mechanical Model of the Piezoelectric Ceramic Tube. Figure 3 shows the mechanical model of the piezoelectric ceramic tube. Here, l_1 is the height of the piezoelectric ceramic tube, $F^1_{r_b}$ is the radial force exerted on the piezoelectric ceramic tube by the metal prestressed tube.

2.1.2. Mechanical Model of the Metal Prestressed Tube. Figure 4 shows the mechanical model of the metal prestressed tube. Here, l_2 is the height of the metal prestressed tube, $F^2_{r_b}$ is the radial force exerted on the metal prestressed tube by the piezoelectric ceramic tube, P_e is the environmental load.

2.2. Mathematical Model. The mathematical model of radial vibration of the transducer is composed of the wave equations of radial vibration of the piezoelectric ceramic tube and the metal prestressed tube, the continuity conditions, and the boundary conditions [19].

In polar coordinates, the wave equation of radial vibration of the piezoelectric ceramic tube is as follows [20]:

$$\rho_1 \frac{\partial^2 u^1}{\partial t^2} = \frac{\partial \sigma_r}{\partial r} + \frac{\sigma_r - \sigma_\theta}{r}, \tag{1}$$

where u^1 is the radial displacement of the piezoelectric ceramic tube, and ρ_1 is the density of the piezoelectric ceramic.

According to the three-dimensional theory of piezoelectric elasticity, when the axial normal stress and the axial shear stress are not considered, the piezoelectric equation is as follows [21]:

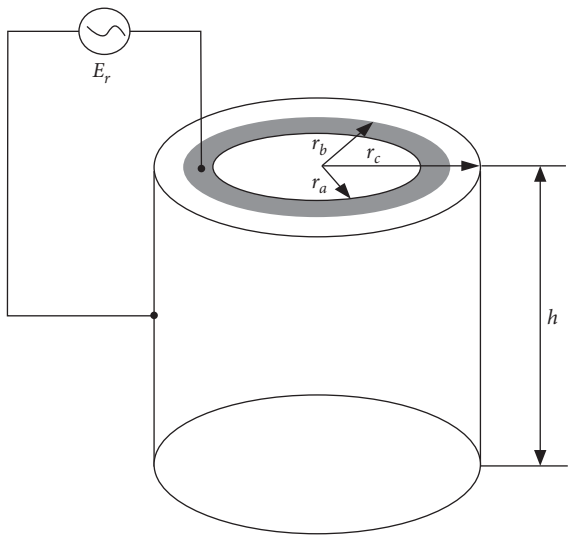

Figure 1: Schematic diagram of the transducer.

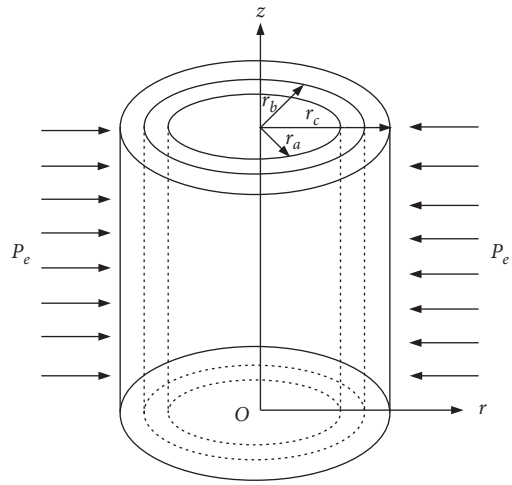

Figure 2: Mechanical model of the transducer.

$$\begin{cases} \varepsilon_r = S_{33}^E \sigma_r + S_{13}^E \sigma_\theta + d_{33} E_r, \\ \varepsilon_\theta = S_{13}^E \sigma_r + S_{11}^E \sigma_\theta + d_{31} E_r, \end{cases} \tag{2}$$

where S_{11}^E, $S_{12}^E S_{13}^E$ and S_{33}^E are elastic compliance coefficients, d_{31} and d_{33} are permittivities, and E_r is the external excitation voltage.

The relationship between strains and displacement is as follows [22]:

$$\begin{aligned} \varepsilon_r &= \frac{\partial u^1}{\partial r}, \\ \varepsilon_\theta &= \frac{u^1}{r}. \end{aligned} \tag{3}$$

The relationship between stresses and displacement can be obtained by combining (2) and (3) are as follows:

$$\begin{cases} \sigma_r = e_{11} \dfrac{\partial u^1}{\partial r} + e_{12} \dfrac{u^1}{r} + e_{13} E_r, \\ \sigma_\theta = e_{12} \dfrac{\partial u^1}{\partial r} + e_{22} \dfrac{u^1}{r} + e_{23} E_r. \end{cases} \tag{4}$$

Here,

$$\begin{cases} e_{11} = \dfrac{S_{11}^E}{S_{11}^E S_{33}^E - S_{13}^E S_{13}^E}, e_{12} = \dfrac{-S_{13}^E}{S_{11}^E S_{33}^E - S_{13}^E S_{13}^E}, \\ e_{13} = \dfrac{S_{13}^E d_{31} - S_{11}^E d_{33}}{S_{11}^E S_{33}^E - S_{13}^E S_{13}^E}, \\ e_{22} = \dfrac{S_{33}^E}{S_{11}^E S_{33}^E - S_{13}^E S_{13}^E}, e_{23} = \dfrac{S_{13}^E d_{33} - S_{33}^E d_{31}}{S_{11}^E S_{33}^E - S_{13}^E S_{13}^E}. \end{cases} \tag{5}$$

By substituting (4) into (1), the wave equation of radial vibration of the piezoelectric ceramic tube can be expressed as follows:

$$\frac{1}{V_1^2} \frac{\partial^2 u^1}{\partial t^2} = \frac{\partial^2 u^1}{\partial r^2} + \frac{1}{r} \frac{\partial u^1}{\partial r} - \frac{e_{22}}{e_{11}} \frac{1}{r^2} u^1 + \frac{e_{13} - e_{23}}{e_{11}} \frac{1}{r} E_r, \tag{6}$$

where $V_1 = \sqrt{e_{11}/\rho_1}$ is the radial propagation velocity of the sound wave in piezoelectric ceramics.

The analysis process of the wave equation of the radial vibration of the metal prestressed tube is the same as that of the piezoelectric ceramic tube. In polar coordinates, the wave equation of radial vibration of the metal prestressed tube is as follows [23]:

$$\rho_2 \frac{\partial^2 u^2}{\partial t^2} = \frac{\partial \sigma_r}{\partial r} + \frac{\sigma_r - \sigma_\theta}{r}, \tag{7}$$

where u^2 is the radial displacement of the piezoelectric ceramic tube, and ρ_2 is the density of metallic material.

According to the thick tube theory [24], the relationship between strains and stresses is as follows:

$$\begin{cases} \varepsilon_r = \dfrac{1}{E_2} [\sigma_r - \gamma_2 \sigma_\theta], \\ \varepsilon_\theta = \dfrac{1}{E_2} [\sigma_\theta - \gamma_2 \sigma_r], \end{cases} \tag{8}$$

where E_2 and γ_2 are the elastic modulus and the Poisson ratio of metallic material.

The relationship between strains and displacement is as follows:

$$\begin{aligned} \varepsilon_r &= \frac{\partial u^2}{\partial r}, \\ \varepsilon_\theta &= \frac{u^2}{r}. \end{aligned} \tag{9}$$

The relationship between stresses and displacement can be obtained by combining (8) and (9) as follows:

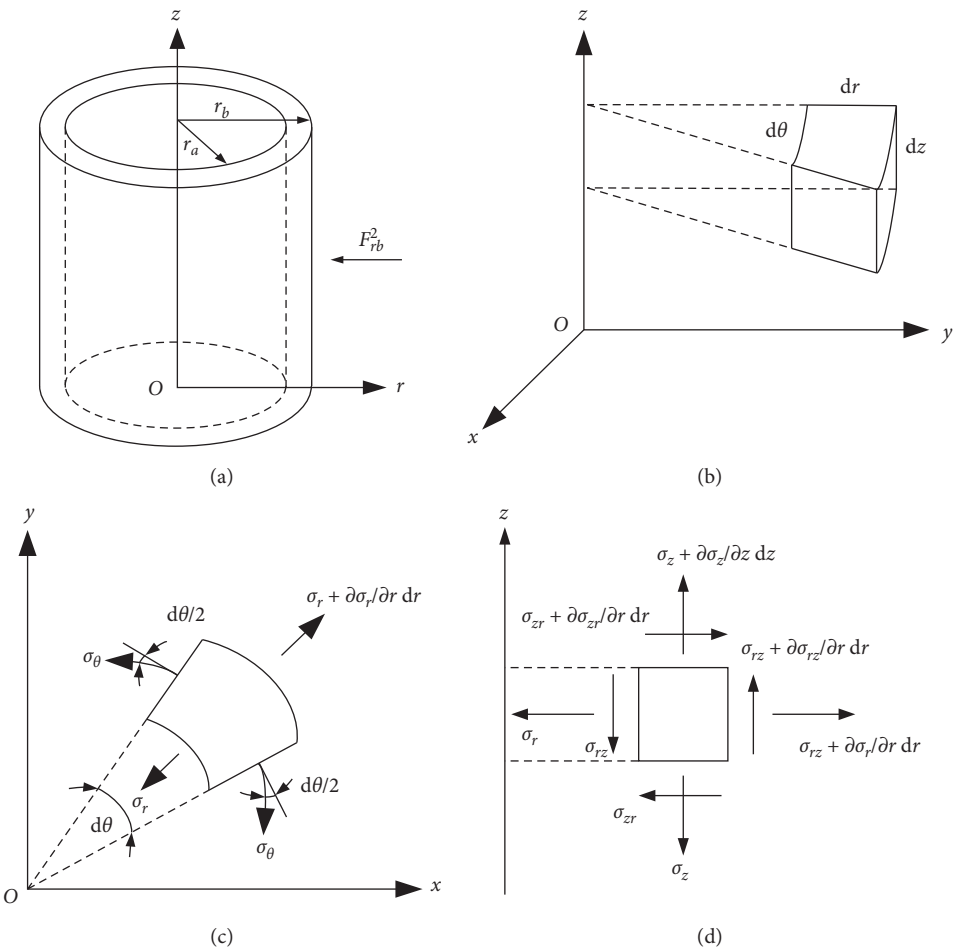

Figure 3: Mechanical model of the piezoelectric ceramic tube: (a) overall stress of piezoelectric ceramic tube, (b) infinitesimal element, (c) $x - y$ plane force, and (d) $r - z$ plane force.

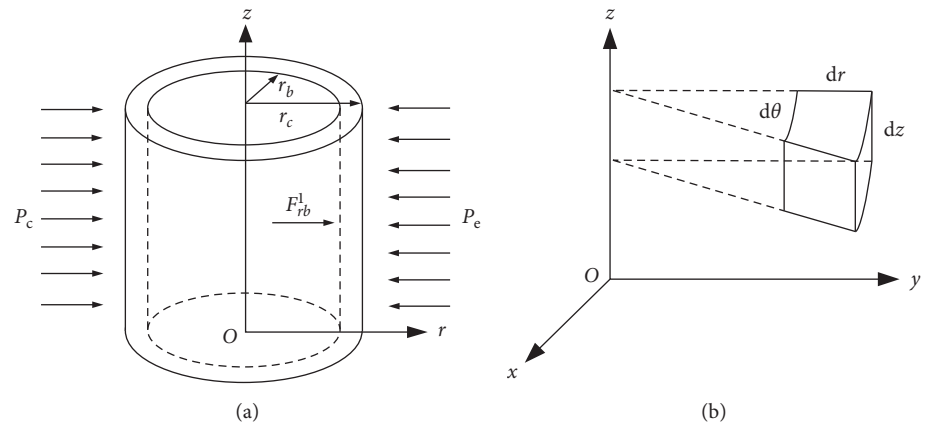

Figure 4: Continued.

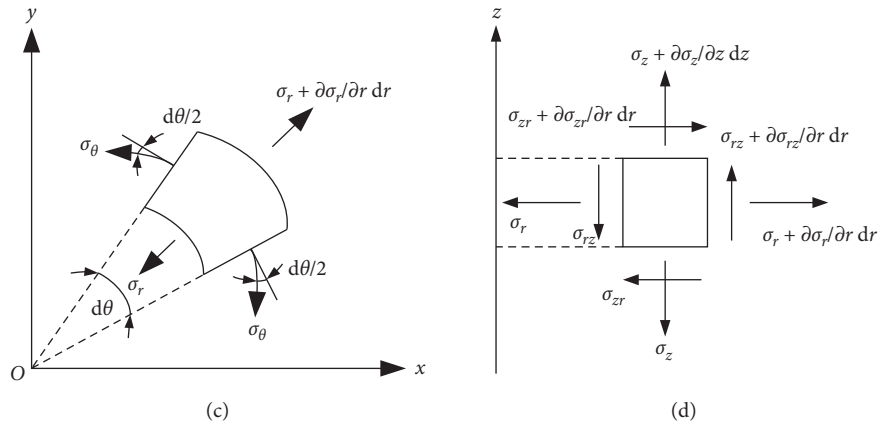

(c) (d)

FIGURE 4: Mechanical model of the metal prestressed tube: (a) overall stress of metal prestressed tube, (b) infinitesimal element, (c) $x - y$ plane force, and (d) $r - z$ plane force.

$$\begin{cases} \sigma_r = c_{11}\dfrac{\partial u^2}{\partial r} + c_{12}\dfrac{u^2}{r}, \\ \sigma_\theta = c_{12}\dfrac{\partial u^2}{\partial r} + c_{11}\dfrac{u^2}{r}. \end{cases} \tag{10}$$

Here,

$$\begin{aligned} c_{11} &= \frac{E_2}{1-\gamma_2^2}, \\ c_{12} &= \frac{E_2\gamma_2}{1-\gamma_2^2}. \end{aligned} \tag{11}$$

By substituting (10) into (7), the wave equation of radial vibration of the metal prestressed tube can be expressed as follows:

$$\frac{1}{V_2^2}\frac{\partial^2 u^2}{\partial t^2} = \frac{\partial^2 u^2}{\partial r^2} + \frac{1}{r}\frac{\partial u^2}{\partial r} - \frac{1}{r^2}u^2, \tag{12}$$

where $V_2 = \sqrt{c_{11}/\rho_2}$ is the radial propagation velocity of the sound wave in metallic materials.

The external boundary condition of the metal prestressed tube is a stress boundary condition. Its external load is environmental pressure:

$$\sigma_r\big|_{r=r_c} = -P_e. \tag{13}$$

The inner boundary condition of the piezoelectric ceramic tube is as follows:

$$\sigma_r\big|_{r=r_a} = 0. \tag{14}$$

The displacement continuity condition and the force continuity condition are as follows:

$$\begin{cases} v(r_b,t) = u(r_b,t), \\ S_1\sigma_{r_b}^1 = S_2\sigma_{r_b}^2, \end{cases} \tag{15}$$

where $S_1 = 2\pi r_b l_1$ and $S_2 = 2\pi r_b l_2$ are the area of piezoelectric ceramic tube outer wall and the metal prestressed tube inner wall, $\sigma_{r_b}^1$ and $\sigma_{r_b}^2$ are the radial stress on the outer surface of the piezoelectric ceramic tube and the inner surface of the metal prestressed tube.

In conclusion, the mathematical model of radial vibration of the transducer can be obtained as follows:

$$\begin{cases} \dfrac{1}{V_1^2}\dfrac{\partial^2 u^1}{\partial t^2} = \dfrac{\partial^2 u^1}{\partial r^2} + \dfrac{1}{r}\dfrac{\partial u^1}{\partial r} - \dfrac{e_{22}}{e_{11}}\dfrac{1}{r^2}u^1 + \dfrac{e_{13}-e_{23}}{e_{11}}\dfrac{1}{r}E_r, \\ \dfrac{1}{V_2^2}\dfrac{\partial^2 u^2}{\partial t^2} = \dfrac{\partial^2 u^2}{\partial r^2} + \dfrac{1}{r}\dfrac{\partial u^2}{\partial r} - \dfrac{1}{r^2}u^2, \\ \sigma_r\big|_{r=r_a} = 0, \\ \sigma_r\big|_{r=r_c} = -P_e, \\ u^1(r_b,t) = u^2(r_b,t), \\ S_1\sigma_{r_b}^1 = S_2\sigma_{r_b}^2. \end{cases} \tag{16}$$

3. Analytical Solution of Radial Vibration of Transducer

3.1. Vibration Mode Function and Natural Frequency. The natural frequency is the inherent property of the object, which is independent of the electric field excitation and the external environment pressure [25]. When the frequency equation needs to be derived, the transducer should be in a free vibration state, and there is no voltage excitation and external environmental pressure.

The separation of displacement functions is done by splitting space and temporal variables [26]. Let $u^1 = u_r^1 e^{j\omega t} u^2 = u_r^2 e^{j\omega t}$, equation (16) can be expressed as follows:

$$\begin{cases} r^2\dfrac{\mathrm{d}^2 u_r^1}{\mathrm{d}r^2} + r\dfrac{\mathrm{d}u_r^1}{\mathrm{d}r} + \left(k_1^2 r^2 - m^2\right)u_r^1 = 0, \\ r^2\dfrac{\mathrm{d}^2 u_r^2}{\mathrm{d}r^2} + r\dfrac{\mathrm{d}u_r^2}{\mathrm{d}r} + \left(k_2^2 r^2 - 1\right)u_r^2 = 0, \end{cases} \tag{17}$$

where ω is the angular frequency, $k_1 = \omega/V_1$ and $k_2 = \omega/V_2$ are the wave numbers of radial vibration of the piezoelectric

ceramic tube vibrator and the metal prestressed tube vibrator, and $m = \sqrt{e_{22}/e_{11}}$.

Equation (18) is a Bessel equation of order 1 and order m [27]. Its general solution is as follows:

$$\begin{cases} u_r^1 = A_1 J_m(k_1 r) + B_1 Y_m(k_1 r), \\ u_r^2 = A_2 J_1(k_2 r) + B_2 Y_1(k_2 r). \end{cases} \tag{18}$$

By substituting equation (19) into the boundary conditions and the continuity conditions, the following conclusions can be drawn.

At the inner diameter of the piezoelectric ceramic tube, the stress boundary condition is as follows:

$$e_{11}\left[A_1 J_m'(k_1 r_a) + B_1 Y_m'(k_1 r_a)\right] + \frac{e_{12}}{r_a} \cdot \left[A_1 J_m(k_1 r_a) + B_1 Y_m(k_1 r_a)\right] = 0. \tag{19}$$

At the outer diameter of the metal prestressed tube, the stress boundary condition is as follows:

$$c_{11}\left[A_2 J_1'(k_2 r_c) + B_2 Y_1'(k_2 r_c)\right] + \frac{c_{12}}{r_c} \cdot \left[A_2 J_1(k_2 r_c) + B_2 Y_1(k_2 r_c)\right] = 0. \tag{20}$$

The displacement continuity condition and the force continuity condition is as follows:

$$\begin{cases} A_1 J_m(k_1 r_b) + B_1 Y_m(k_1 r_b) = A_2 J_1(k_2 r_b) + B_2 Y_1(k_2 r_b), \\ S_1 e_{11}\left[A_1 J_m'(k_1 r_b) + B_1 Y_m'(k_1 r_b)\right] + \frac{e_{12}}{r_b}\left[A_1 J_m(k_1 r_b) + B_1 Y_m(k_1 r_b)\right], \\ = S_2 c_{11}\left[A_2 J_1'(k_2 r_b) + B_2 Y_1'(k_2 r_b)\right] + S_2 \frac{c_{12}}{r_b}\left[A_2 J_1(k_2 r_b) + B_2 Y_1(k_2 r_b)\right]. \end{cases} \tag{21}$$

The characteristic equation of radial vibration of the transducer can be obtained by combining (20), (21), and (22):

$$S_1 \frac{[e_{11} Y_m'(k_1 r_b) + (e_{12}/r_b) Y_m(k_1 r_b)] - [e_{11} J_m'(k_1 r_b) + (e_{12}/r_b) J_m(k_1 r_b)]\left([e_{11} Y_m'(k_1 r_a) + (e_{12}/r_b) Y_m(k_1 r_a)]/[e_{11} J_m'(k_1 r_a) + (e_{12}/r_b) J_m(k_1 r_a)]\right)}{Y_m(k_1 r_b) - J_m(k_1 r_b)\left([e_{11} Y_m'(k_1 r_b) + (e_{12}/r_b) Y_m(k_1 r_a)]/[e_{11} J_m'(k_1 r_a) + (e_{12}/r_b) J_m(k_1 r_a)]\right)}$$
$$= S_2 \frac{[c_{11} Y_1'(k_2 r_b) + (c_{12}/r_b) Y_1(k_2 r_b)] - [c_{11} J_1'(k_2 r_b) + (c_{12}/r_b) J_1(k_2 r_b)]\left([c_{11} Y_1'(k_2 r_c) + (c_{12}/r_b) Y_1(k_2 r_c)]/[c_{11} J_1'(k_2 r_c) + (c_{12}/r_b) J_1(k_2 r_c)]\right)}{Y_1(k_2 r_b) - J_1(k_2 r_b)\left([c_{11} Y_1'(k_2 r_c) + (c_{12}/r_b) Y_1(k_2 r_c)]/[c_{11} J_1'(k_2 r_c) + (c_{12}/r_b) J_v(k_2 r_c)]\right)}. \tag{22}$$

The natural frequency can be calculated by the characteristic equation [28]. The computing method is as follows:

$$f_n = \omega_n / 2\pi, \quad (n = 1, 2, 3, \ldots). \tag{23}$$

It can be obtained by combining (20)–(22):

$$A_1 = -\frac{[e_{11} Y_m'(k_1 r_a) + (e_{12}/r_a) Y_m(k_1 r_a)]}{[e_{11} J_m(k_1 r_a) + (e_{12}/r_a) J_m(k_1 r_a)]} B_1,$$

$$A_2 = -\frac{[c_{11} Y_1'(k_2 r_c) + (c_{12}/r_b) Y_1(k_2 r_c)]}{[c_{11} J_1'(k_2 r_c) + (c_{12}/r_b) J_1(k_2 r_c)]} B_2,$$

$$\frac{B_1}{B_2} = \frac{Y_1(k_2 r_b) - J_1(k_2 r_b)\left([c_{11} Y_1'(k_2 r_c) + (c_{12}/r_c) Y_1(k_2 r_c)]/[c_{11} J_1'(k_2 r_c) + (k_1 r_a) J_v(k_2 r_c)]\right)}{Y_m(k_1 r_b) - J_m(k_1 r_b)\left([e_{11} Y_m'(k_1 r_a) + (e_{12}/r_a) Y_m(k_1 r_a)]/[e_{11} J_m'(k_1 r_a) + (e_{12}/r_a) J_m(k_1 r_a)]\right)}$$
$$= \frac{S_2[c_{11} Y_1'(k_2 r_b) + (c_{12}/r_b) Y_1(k_2 r_b)] - [c_{11} J_1'(k_2 r_b) + (c_{12}/r_b) J_1(k_2 r_b)]\left([c_{11} Y_1'(k_2 r_c) + (c_{12}/r_c) Y_1(k_2 r_c)]/[c_{11} J_1'(k_2 r_c) + (c_{12}/r_c) J_1(k_2 r_c)]\right)}{S_1[e_{11} Y_m'(k_1 r_b) + (e_{12}/r_b) Y_m(k_1 r_b)] - [e_{11} J_m'(k_1 r_b) + (e_{12}/r_b) J_m(k_1 r_b)]\left([e_{11} Y_m'(k_1 r_a) + (e_{12}/r_a) Y_m(k_1 r_a)]/[e_{11} J_m'(k_1 r_a) + (e_{12}/r_a) J_m(k_1 r_a)]\right)}. \tag{24}$$

Therefore, the mode function is as follows:

$$\begin{cases} u_{rn}^{1} = \dfrac{Y_1(k_{2n}r_b) - J_1(k_{2n}r_b)\left([c_{11}Y_1'(k_{2n}r_c) + (c_{12}/r_c)Y_1(k_{2n}r_c)]/[c_{11}J_1'(k_{2n}r_c) + (c_{12}/r_c)J_1(k_{2n}r_c)]\right)}{Y_m(k_{1n}r_b) - J_m(k_{1n}r_b)\left([e_{11}Y_m'(k_{1n}r_a) + (e_{12}/r_a)Y_m(k_{1n}r_a)]/[e_{11}J_m'(k_{1n}r_a) + (e_{12}/r_a)J_m(k_{1n}r_a)]\right)} \\ \quad \left[\dfrac{e_{11}Y_m'(k_{1n}r_a) + (e_{12}/r_b)Y_m(k_{1n}r_a)}{e_{11}J_m'(k_{1n}r_a) + (e_{12}/r_b)J_m(k_{1n}r_a)}J_m(k_{1n}r) + Y_m(k_{1n}r)\right], \\ u_{rn}^{2} = -\dfrac{[c_{11}Y_1'(k_{2n}r_c) + (c_{12}/r_c)Y_1(k_{2n}r_c)]}{[c_{11}J_1'(k_{2n}r_c) + (c_{12}/r_c)J_1(k_{2n}r_c)]}J_1(k_{2n}r) + Y_1(k_{2n}r). \end{cases} \tag{25}$$

4. Displacement

4.1. Analytical Solution. Let $u^1 = u_r^1 e^{j\omega t}$, $u^2 = u_r^2 e^{j\omega t}$, and $E_r = E_0 e^{j\omega t}$; equation (17) can be expressed as follows:

$$\begin{cases} r^2\dfrac{\mathrm{d}^2u_r^1}{\mathrm{d}r^2} + r\dfrac{\mathrm{d}u_r^1}{\mathrm{d}r} + \left(k_1^2r^2 - m^2\right)u_r^1 + \dfrac{\mathrm{e}_{13} - e_{23}}{e_{11}}E_0 = 0, \\ r^2\dfrac{\mathrm{d}^2u_r^2}{\mathrm{d}r^2} + r\dfrac{\mathrm{d}u_r^2}{\mathrm{d}r} + \left(k_2^2r^2 - 1\right)u_r^2 = 0. \end{cases} \tag{26}$$

Equation (26) is the Bessel equation and Lommel equation. Its general solution is as follows:

$$\begin{cases} u_r^1 = H_1J_m(k_1r) + G_1Y_m(k_1r) + \dfrac{\mathrm{e}_{23} - e_{13}}{e_{11}}E_0S_{0,m}(k_1r), \\ u_r^2 = H_2J_1(k_2r) + G_2Y_1(k_2r). \end{cases} \tag{27}$$

The boundary conditions and continuity conditions can be expressed as follows:

$$\begin{aligned} & e_{11}\left[H_1J_m'(k_1r_a) + G_1Y_m'(k_1r_a)\right] + \frac{e_{12}}{r_a}\left[H_1J_m(k_1r_a) + G_1Y_m(k_1r_a)\right] \\ & \quad + \left[(e_{23} - e_{13})S_{0,v}'(k_1r_a) + \frac{e_{12}}{r_a}\frac{(e_{23} - e_{13})}{e_{11}}S_{0,m}(k_1r_a) + e_{13}\right]E_0 = 0, \\ & c_{11}\left[H_2J_1'(k_2r_c) + G_2Y_1'(k_2r_c)\right] + \frac{c_{12}}{r_c}\left[H_2J_1(k_2r_c) + G_2Y_1(k_2r_c)\right] = -P_e, \\ & H_1J_m(k_1r_b) + G_1Y_m(k_1r_b) + \frac{e_{23} - e_{13}}{e_{11}}E_0S_{0,m}(k_1r_b) = H_2J_1(k_2r_b) + G_2Y_1(k_2r_b), \\ & S_1e_{11}\left[H_2J_m'(k_1r_b) + G_1Y_m'(k_1r_b)\right] + \frac{e_{12}}{r_b}\left[H_1J_m(k_1r_b) + G_1Y_m(k_1r_b)\right] \\ & \quad + S_1\left[(e_{23} - e_{13})S_{0,m}'(k_1r_a) + \frac{e_{12}}{r_a}\frac{(e_{23} - e_{13})}{e_{11}}S_{0,m}(k_1r_a) + e_{13}\right]E_0 \\ & \quad = S_2c_{11}\left[H_2J_1'(k_2r_b) + G_2Y_1'(k_2r_b)\right] + S_2\frac{c_{12}}{r_b}\left[H_2J_1(k_2r_b) + G_2Y_1(k_2r_b)\right]. \end{aligned} \tag{28}$$

According to the boundary conditions and the continuity conditions, the response of the system is as follows:

$$\begin{cases} u^1(r,t) = \left[H_1J_m(k_1r) + G_1Y_m(k_1r) + \dfrac{e_{23} - e_{13}}{e_{11}}E_0S_{0,m}(k_1r)\right]e^{j\omega t}, \\ u^2(r,t) = \left[H_2J_1(k_2r) + G_2Y_1(k_2r)\right]e^{j\omega t}. \end{cases} \tag{29}$$

Here,

$$
\begin{aligned}
G_1 &= \frac{F_{22}}{F_{21}}G_2 + \frac{F_{23}}{F_{21}},\\
G_2 &= \frac{(F_{23}/F_{21}) - (F_{13}/F_{11})}{(F_{12}/F_{11}) - (F_{22}/F_{21})},\\
H_1 &= -\frac{[e_{11}Y_m'(k_1r_a) + (e_{12}/r_b)Y_m(k_1r_a)]}{[e_{11}J_m'(k_1r_a) + (e_{12}/r_b)J_m(k_1r_a)]}G_1 - \frac{\left[(e_{23}-e_{13})E_0S_{0,m}'(k_1r_a) + (e_{12}/e_{11})(e_{23}-e_{13}/r_a)E_0S_{0,m}(k_1r_a) + e_{13}E_0\right]}{[e_{11}J_m'(k_1r_a) + (e_{12}/r_b)J_m(k_1r_a)]},\\
H_2 &= -\frac{[c_{11}Y_1'(k_2r_c) + (c_{12}/r_b)Y_1(k_2r_c)]}{[c_{11}J_1'(k_2r_c) + (c_{12}/r_b)J_1(k_2r_c)]}G_2 - \frac{P_e}{[c_{11}J_1'(k_2r_c) + (c_{12}/r_b)J_1(k_2r_c)]},\\
F_{11} &= Y_m(k_1r_b) - J_m(k_1r_b)\frac{[e_{11}Y_m'(k_1r_a) + (e_{12}/r_b)Y_m(k_1r_a)]}{[e_{11}J_m'(k_1r_a) + (e_{12}/r_b)J_m(k_1r_a)]},\\
F_{21} &= S_1[e_{11}Y_m'(k_1r_b) + (e_{12}/r_b)Y_m(k_1r_b)] - S_1[e_{11}J_m'(k_1r_b) + (e_{12}/r_b)J_m(k_1r_b)]\frac{[e_{11}Y_m'(k_1r_a) + (e_{12}/r_b)Y_m(k_1r_a)]}{[e_{11}J_m'(k_1r_a) + (e_{12}/r_b)J_m(k_1r_a)]},\\
F_{12} &= Y_1(k_2r_b) - J_1(k_2r_b)\frac{[c_{11}Y_1'(k_2r_c) + (c_{12}/r_b)Y_1((k_2r_c)]}{[c_{11}J_1'(k_2r_c) + (c_{12}/r_b)J_1(k_2r_c)]},\\
F_{22} &= S_2[c_{11}Y_1'(k_2r_b) + (c_{12}/r_b)Y_1(k_2r_b)] - S_2[c_{11}J_1'(k_2r_b) + (c_{12}/r_b)J_1(k_2r_b)]\frac{[c_{11}Y_1'(k_2r_c) + (c_{12}/r_b)Y_1(k_2r_c)]}{[c_{11}J_1'(k_2r_c) + (c_{12}/r_b)J_1(k_2r_c)]},\\
F_{13} &= \frac{e_{23}-e_{13}}{e_{11}}E_0S_{0,m}(k_1r_a) - \frac{\left[(e_{23}-e_{13})_0S_{0,m}'(k_1r_a) + (e_{12}/e_{11})(e_{23}-e_{13}/r_a)E_0S_{0,m}(k_1r_a) + e_{13}E_0\right]}{[e_{11}J_m'(k_1r_a) + (e_{12}/r_b)J_m(k_1r_a)]}\\
&\quad + J_1(k_2r_b)\frac{P_e}{[c_{11}J_1'(k_2r_c) + (c_{12}/r_b)J_1(k_2r_c)]},\\
F_{23} &= S_1\left[(e_{23}-e_{13})E_0S_{0,m}'(k_1r_b) + \frac{e_{12}}{e_{11}}\frac{e_{23}-e_{13}}{r_b}E_0S_{0,m}(k_1r_b) + e_{13}E_0\right]\\
&\quad - S_1\frac{[e_{11}J_m'(k_1r_b) + (e_{12}/r_b)J_m(k_1r_b)]}{[e_{11}J_m'(k_1r_b) + (e_{12}/r_b)J_m(k_1r_b)]}S_2\left[(e_{23}-e_{13})E_0S_{0,m}'(k_1r_a) + \frac{e_{12}}{e_{11}}\frac{e_{23}-e_{13}}{r_b}E_0S_{0,m}(k_1r_a) + e_{13}E_0\right]\\
&\quad + S_2\left[c_{11}J_1'(k_1r_b) + \frac{c_{12}}{r_b}J_1(k_1r_b)\right]\frac{P_e}{[c_{11}J_1'(k_2r_c) + (c_{12}/r_b)J_1(k_2r_c)]}.
\end{aligned}
\tag{30}
$$

4.2. Difference Solution. The transducer is discretized along the radial direction. The plane $r - z$ is the research plane, the transducer is divided into I nodes along the radial direction, and the unit length is dr. The inner wall of the piezoelectric ceramic tube is the first node, the outer wall of the metal prestressed tube is the node I, and the composite position is the node i_0. Figure 5 shows the discrete model of the radial vibration of the transducer. Time is divided into $J + 1$ time nodes. $u_{i,j}$, $(i = 0, 1, 2, 3, \ldots, I)$ represents the radial vibration displacement of the i space node at the j time node.

The numerical simulation model can be obtained by using the forward difference formula and the central difference formula [29].

The difference equations are as follows:

$$
\begin{aligned}
u_{i,j+1}^1 &= v_2^2\Delta t^2\begin{bmatrix}(1/\Delta r^2)\left(u_{i+1,j} - 2u_{i,j} + u_{i-1,j}\right) + \left(1/\left(r_a + i\Delta r\right)\Delta r\right)\left(u_{i+1,j} - u_{i,j}\right)\\ -(e_{22}/e_{11})\left(1/\left(r_a + i\Delta r\right)^2\right)u_{i,j} + \left(e_{13} - e_{23}/e_{11}\right)\left(1/\left(r_a + i\Delta r\right)\right)\left(E_r\right)_{j+1}\end{bmatrix} + 2u_{i,j} - u_{i,j-1},\\
u_{i,j+1} &= v_2^2\Delta t^2\begin{bmatrix}(1/\Delta r^2)\left(u_{i+1,j} - 2u_{i,j} + u_{i-1,j}\right) + \left(1/\left(r_a + i\Delta r\right)\Delta r\right)\left(u_{i+1,j} - u_{i,j}\right)\\ -(e_{22}/e_{11})\left(1/\left(r_a + i\Delta r\right)^2\right)u_{i,j} + \left(e_{13} - e_{23}/e_{11}\right)\left(1/\left(r_a + i\Delta r\right)\right)\left(E_r\right)_{j+1}\end{bmatrix} + 2u_{i,j} - u_{i,j-1}.
\end{aligned}
\tag{31}
$$

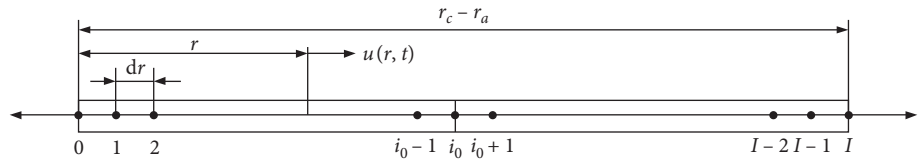

Figure 5: Discrete model of radial vibration of the transducer.

The difference form of the boundary conditions is as follows:

$$u_{0,j+1} = \left[\frac{1}{(e_{11}/\Delta r) - (e_{12}/r_a)}\right]\left[\frac{e_{11}}{\Delta r}u_{1,j+1} + e_{13}(E_r)_{j+1}\right],$$
$$u_{I,j+1} = \left[\frac{1}{(c_{11}/\Delta r) - (c_{12}/r_c)}\right]\frac{c_{11}}{\Delta r}u_{I-1,j+1}. \quad (32)$$

The difference equation of the composite position is as follows:

$$u_{i_0,j+1} = \frac{\left\{\left[S_1c_{11}((1/\Delta r) - (1/2r_b))v_{i_0+1,j} + \left[\begin{array}{c} S_1c_{11}((1/2r_b) - (1/\Delta r) + (\Delta r/2r_b^2)) - S_2e_{11}((1/\Delta r) - (1/2r_b) + (\Delta re_{22}/2e_{11}r_b^2)) \\ -S_2(e_{12}/r_b) + S_1(c_{12}/r_b) \end{array}\right]u_{i_0,j} - S_2e_{11}((1/2r_b) - (1/\Delta r))u_{i_0-1,j} - S_2e_{13}(E_r)_{j+1}\right]\right\}}{[(1/2)\Delta r(1/\Delta t^2)(S_2e_{11}(1/v_1^2) - S_1c_{11}(1/v_2^2))]}. \quad (33)$$

The initial displacement and velocity are 0. The difference form of the initial conditions is as follows:

$$u_{i,0}^1 = 0,$$
$$u_{i,0}^2 = 0,$$
$$u_{i,1}^1 = \frac{1}{2}u_{i,2}, \quad (34)$$
$$u_{i,1}^2 = \frac{1}{2}u_{i,2}^2.$$

Based on the numerical simulation model established above, the difference grid as shown in Figure 6 can be established.

As shown in Figure 6, rectangle "a" represents the numerical calculation path of the inner boundary (the first node) of the difference method: the displacement of the first node is calculated from the second node by the difference form of the inner condition. Rectangle "b" represents the numerical calculation path of the outer boundary (the last node): the displacement of the last node is calculated from the previous node by the difference form of the outer condition. Rectangle "c" and "d" represent the numerical calculation path of internal nodes: the displacement of an internal node is calculated by the displacement of three nodes at the previous time node and one node at the previous two-time node.

5. Example Analysis

The material of the piezoelectric ceramic tube is PZT-4. Its material parameters are as follows: $\rho_1 = 7500\,\text{kg/m}^3$, $S_{11}^E = 12.3 \times 10^{-12}\,\text{m}^2/\text{N}$, $S_{12}^E = -4.05 \times 10^{-12}\,\text{m}^2/\text{N}$, $S_{13}^E = -5.31 \times 10^{-12}\,\text{m}^2/\text{N}$, and $S_{33}^E = 1.55 \times 10^{-12}\,\text{m}^2/\text{N}$. The material of the metal prestressed tube is aluminum alloy. Its material parameters are as follows: $\rho_2 = 2700\,\text{kg/m}^3$, $E_2 = 7.15 \times 10^{10}\,\text{N/m}^3$, and $\gamma_2 = 0.34$.

In order to verify the correctness of the simulation models, the above transducer is calculated as an example.

5.1. Natural Frequency Calculation. The natural frequencies of the three groups of transducers are solved by using the characteristic equation (23), which is also compared with the existing experimental results in reference [13]. As shown in Table 1, the theoretical calculating values f_t are in good agreement with the existing experimental results f_e in the reference, and the accuracy of the obtained characteristic equation meets the requirements of engineering design.

5.2. Amplitude-Frequency Characteristics and Displacement Response. When the excitation frequency of the external voltage is consistent with the natural frequency of the transducer, the transducer will resonate, and its displacement response will suddenly increase [30]. Based on the resonance method, the amplitude-frequency characteristics of the analytical solution and the difference solution are given, respectively.

The structure sizes of the transducer are as follows: $r_a = 21\,\text{mm}, r_b = 26\,\text{mm}, r_c = 31\,\text{mm}, l_1 = l_2 = 34\,\text{mm}$. A 50 V AC voltage is applied to this transducer. For the analytical solution and the difference solution, the amplitude-frequency characteristics of the transducer at 1.2×10^{-5}s are obtained by iteration in 1 Hz step.

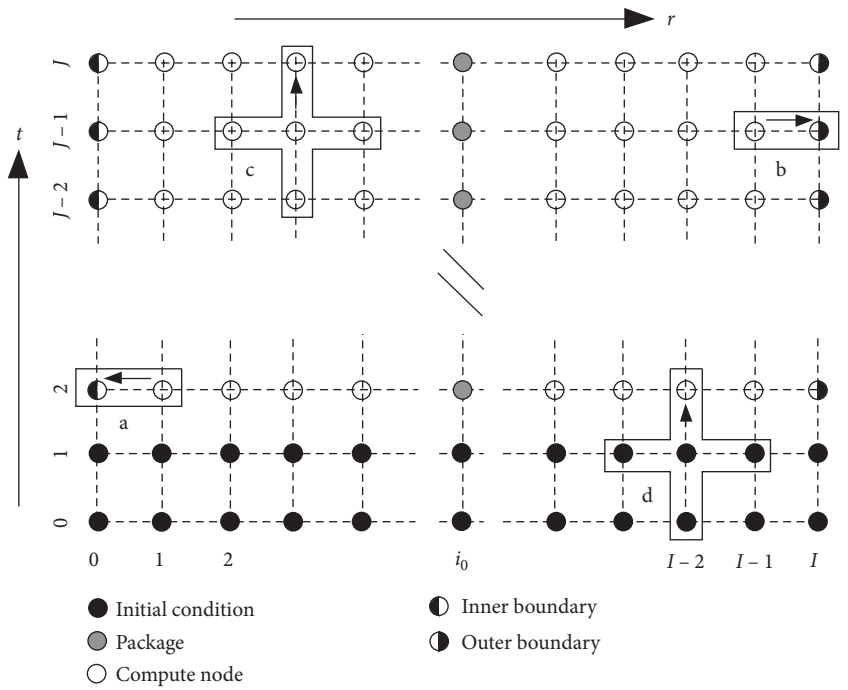

Figure 6: Difference grid.

Table 1: Theoretical and existing values in the reference.

No.	r_a (mm)	r_b (mm)	r_c (mm)	l_1, l_2 (mm)	f_t (Hz)	f_e (Hz)	Δ (%)
1	11	15	21	34	42833	43042	0.48
2	21	26	31	34	24597	25621	3.99
3	50	58	63	84	10704	10851	1.88

Figure 7 shows the frequency characteristic curve of the analytical solution. It can be observed from Figure 7 that the displacement suddenly increases when the frequency of the voltage of the transducer is 24597 Hz. It can be concluded that the natural frequency of the radial vibration of the transducer is 24597 Hz, which meets the value obtained by the characteristic equation.

Limited by the time length and the accuracy of computer calculation, let $dt = 3 \times 10^{-9}$ s, $dr = 5 \times 10^{-5}$ m. The amplitude-frequency characteristic of the difference solution at 1.2×10^{-5} s can be obtained by calculating the 4000th time node and the 101st space node. Figure 8 shows the frequency characteristic curve of the difference solution. It can be concluded that the natural frequency of the radial vibration of the transducer is 24597 Hz, which is consistent with the conclusion of the characteristic equation and the analytical solution.

For the transducer of the same structure sizes, when a radial excitation voltage of 20000 Hz and 50 V is applied to the transducer, the displacement responses of the analytical solution and the differential solution are as shown in Figure 9.

It can be observed from Figure 9 that the radial vibration displacement curves obtained by the analytical method, and the difference method are same when the transducer with same structure sizes and same external excitation voltage, which realizes the mutual verification between the analytical solution and the differential solution of radial vibration of the transducer and proves the correctness of the simulation result.

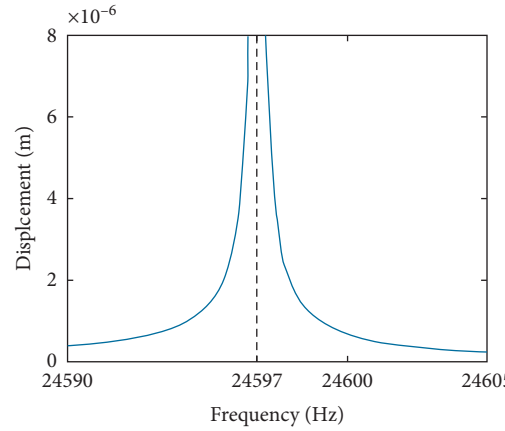

Figure 7: Amplitude-frequency characteristics of the analytical solution.

6. Relationship between Natural Frequencies and Structural Dimensions

Continuum mechanics models depicted that thickness plays a significant role for vibrational analysis of tubes [31, 32].

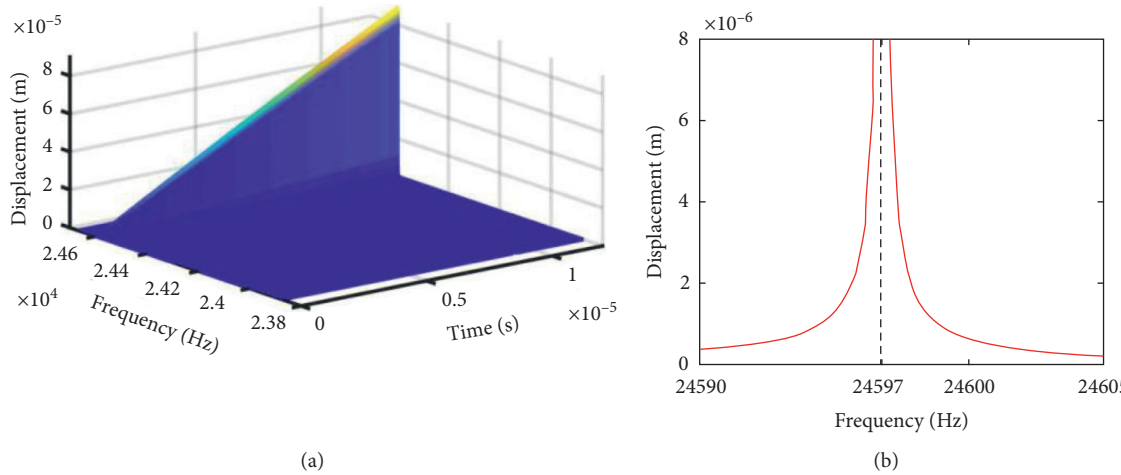

Figure 8: Amplitude-frequency characteristics of the difference solution: (a) there-dimensional diagram; (b) the amplitude-frequency characteristics.

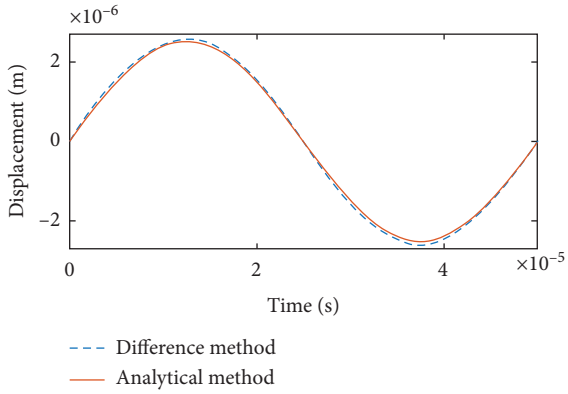

Figure 9: Displacement.

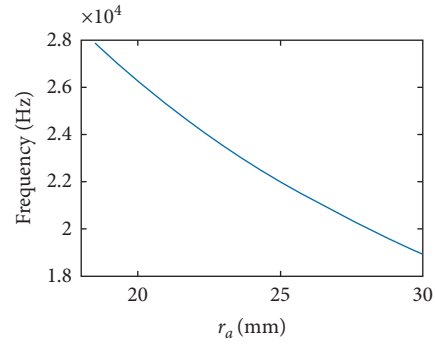

Figure 10: Relationship between natural frequency and inner diameter

Taking the transducer of metal prestressed tube as steel and piezoelectric ceramic tube as PZT-4 as an example, the relationship between natural frequency and structure sizes is given by programming with MATLAB.

Its material parameters are as follows:$\rho_1 = 7500\,\text{kg/m}^3$, $\rho_2 = 7930\,\text{kg/m}^3$, $E_2 = 209 \times 10^{10}\,\text{N/m}^3$, $\gamma_2 = 0.28$, $S_{11}^E = 12.3 \times 10^{-11}\,\text{m}^2/\text{N}$, $S_{12}^E = -4.05 \times 10^{-11}\,\text{m}^2/\text{N}$, $S_{13}^E = -5.31 \times 10^{-12}\,\text{m}^2/\text{N}$, and $S_{33}^E = 1.55 \times 10^{-12}\,\text{m}^2/\text{N}$.

Keep the wall thickness of the piezoelectric ceramic tube and the metal prestressed tube as 5 mm, and take the inner diameter of the piezoelectric ceramic tube as 18–30 mm. Other structure sizes are as follows:$l_1 = 40$ mm, $l_2 = 30$ mm. For the above group of transducers, the relationship curve between the natural frequency and the inner diameter obtained by using the derived characteristic equation is as shown in Figure 10. It can be observed from Figure 10, when the wall thickness of the metal prestressed tube and the piezoelectric ceramic tube is kept constant, the larger the inner diameter of the piezoelectric ceramic tube, the smaller the natural frequency of radial vibration of the transducer.

Keep the wall thickness of the piezoelectric ceramic tube and the metal prestressed tube, the outer diameter of the metal prestressed tube, and the inner diameter of the piezoelectric ceramic tube unchanged. The only change is the inner diameter of the metal prestressed tube or the outer diameter of the piezoelectric ceramic tube. The thickness-to-wall ratio $\lambda = (r_b - r_a)/(r_c - r_a)$ is introduced, which represents the proportion of the thickness of the piezoelectric ceramic tube to the total thickness of the transducer. When λ is 0, the transducer becomes a metal prestressed tube, and when λ is 1, the transducer becomes a piezoelectric ceramic tube. The relationship between the natural frequency and the thickness-to-wall ratio can be obtained by using the derived characteristic equation.

Figure 11 shows the relationship between the natural frequency and the wall thickness-to-wall ratio. It can be observed from Figure 11 that the natural frequency decreases with the increase of the thickness-to-wall ratio. The reason is that the elastic modulus of piezoelectric ceramic material is smaller than that of metal material. The larger thickness of the piezoelectric ceramic tube equates with the larger proportion of piezoelectric ceramic material in the transducer, so the natural frequency will decrease.

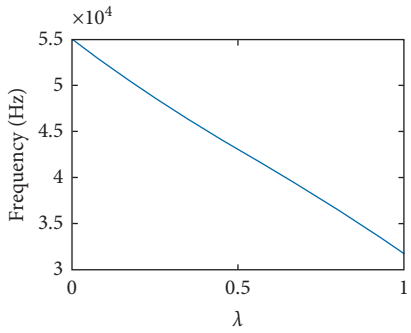

Figure 11: Relationship between natural frequency and wall thickness ratio.

7. Conclusions

(1) The focus in the paper is on the radial vibration characteristics of the piezoelectric ceramic composite ultrasonic transducer. The transducer is simplified as a mechanical model of a composite thick wall tube composed of a piezoelectric ceramic tube and a metal prestressed tube. The mathematical model of radial vibration of the transducer is established, which consists of the wave equation of radial coupling vibration of the piezoelectric ceramic tube and the metal prestressed tube, the continuity conditions, and the boundary conditions of radial vibration of composite thick wall tube. The characteristic equation and the mode function of the radial vibration of the transducer are obtained. The results of natural frequency calculations are consistent with the existing experimental results, which proves the correctness of the simulation models and the accuracy of the obtained characteristic equation meets the requirement of engineering design.

(2) Based on the analytical method and the difference method, the numerical simulation models of radial vibration of the transducer are established, and the amplitude-frequency characteristic curves and the displacement responses of radial vibration of the transducer are given. The simulation results show that the amplitude-frequency characteristic curves and the displacement responses of the two methods are the same, which verifies the correctness of the simulation results.

(3) The relationship between the natural frequency and the transducer's structural sizes are obtained: when the thickness of the metal prestressed tube and the piezoelectric ceramic tube are constant, the natural frequency decreases with the increase of the inner diameter of the piezoelectric ceramic tube. And when the outer diameter of the metal prestressed tube and the inner diameter of the piezoelectric ceramic tube are constant, the natural frequency decreases with the increase of the thickness-to-wall ratio.

(4) The theory in this paper is based on the vibration theory of the mechanical system and combined with the constitutive equation. This method can be used to analyze the radial vibration characteristics of the transducer composed of a piezoelectric ceramic ring (tube) and an outer metal ring (tube). Compared with the current analysis method of radial vibration characteristics of the transducer based on the equivalent circuit, the calculation method of natural frequency based on elastic vibration theory is clear in concept and simple in calculation, and the simulation model can analyze the mechanical vibration of the transducer. This method has a guiding significance for the design of the piezoelectric ceramic composite ultrasonic transducer.

Data Availability

The data used to support the findings of this study are available from the corresponding author upon request.

Conflicts of Interest

The authors declare that they have no conflicts of interest regarding the publication of this work.

Acknowledgments

The authors would like to thank the National Natural Science Foundation of China (Grant No. 51974276) for funding.

References

[1] K. Uchino, "Glory of piezoelectric perovskites," *Science and Technology of Advanced Materials*, vol. 16, p. 4, 2015.

[2] S. Lin, "Study on the Langevin piezoelectric ceramic ultrasonic transducer of longitudinal-flexural composite vibrational mode," *Ultrasonics*, vol. 44, no. 1, pp. 109–114, 2006.

[3] D. Chacón, G. Rodrı´guez-Corral, L. Gaete-Garretón, E. Riera-Franco de Sarabia, and J. A. Gallego-Juárez, "A procedure for the efficient selection of piezoelectric ceramics constituting high-power ultrasonic transducers," *Ultrasonics*, vol. 44, no. 1, pp. e517–e521, 2006.

[4] S. W. Or, H. L. W. Chan, and P. C. K. Liu, "Piezocomposite ultrasonic transducer for high-frequency wire-bonding of microelectronics devices," *Sensors and Actuators A: Physical*, vol. 133, no. 1, pp. 195–199, 2007.

[5] F. J. Arnold and S. S. Mühlen, "The resonance frequencies on mechanically pre-stressed ultrasonic piezotransducers," *Ultrasonics*, vol. 39, no. 1, pp. 1–5, 2001.

[6] S. L. Peshkovsky and A. S. Peshkovsky, "Matching a transducer to water at cavitation: acoustic horn design principles," *Ultrasonics Sonochemistry*, vol. 14, no. 3, pp. 314–322, 2007.

[7] S. Lin, "The radial composite piezoelectric ceramic transducer," *Sensors and Actuators A: Physical*, vol. 141, no. 15, pp. 136–143, 2008.

[8] S. Lin Shuyu and S. Wang Shuaijun, "Radially composite piezoelectric ceramic tubular transducer in radial vibration," *IEEE Transactions on Ultrasonics, Ferroelectrics and Frequency Control*, vol. 58, no. 11, pp. 2492–2498, 2011.

[9] Y. Shui and Q. Xue, "Dynamic characteristics of 2-2 piezoelectric composite transducers," *IEEE Transactions on*

Ultrasonics, Ferroelectrics, and Frequency Control, vol. 44, no. 5, pp. 1110–1119, 1997.

[10] W. Manthey, N. Kroemer, and V. Magori, "Ultrasonic transducers and transducer arrays for applications in air," *Measurement Science and Technology*, vol. 3, no. 3, pp. 249–261, 1999.

[11] S. Liu and W. Yao, "Radial vibration characteristics of composite pipe power piezoelectric ultrasonic transducer," *Chinese Journal of Mechanical Engineering*, vol. 44, no. 10, pp. 239–244, 2008.

[12] S. Liu and S. Lin, "The analysis of the electro-mechanical model of the cylindrical radial composite piezoelectric ceramic transducer," *Sensors and Actuators A: Physical*, vol. 155, no. 1, pp. 175–180, 2009.

[13] S. Lin, S. Wang, and Z. Fu, "Radial vibration for a radially polarized piezoelectric composite transducer," *Acta Acustica*, vol. 38, no. 3, pp. 354–363, 2013.

[14] L. Li, S. Liu, and L. Dan, "Radial vibration of a regular polygon composite piezoelectric ultrasonic transducer," *Journal of Mechanical Engineering*, vol. 52, no. 15, pp. 22–26, 2016.

[15] L. Jia, G. Zhang, X. Zhang, Y. Yao, and S. Lin, "Study on tangentially polarized composite cylindrical piezoelectric transducer with high electro-mechanical coupling coefficient," *Ultrasonics*, vol. 74, pp. 204–210, 2017.

[16] Li Guo, J. Gong, and T. Wang, "Study on the broadband piezoelectric ceramic transducer based on radial enhanced-composite structure," *Ceramics International*, vol. 44, pp. 250–253, 2018.

[17] W. S. Abushanab, "Inexpensive pipelines health evaluation techniques based on resonance determination, numerical simulation and experimental testing," *Engineering*, vol. 5, no. 4, pp. 337–343, 2013.

[18] X. Li, "Complete plane strain problem of a nonhomogeneous elastic body with a doubly-periodic set of cracks," *Zamm*, vol. 81, no. 6, pp. 377–391, 2001.

[19] X. Sun, S. Dong, W. Li, and W. Zhang, "The numerical simulation of entire sucker rod string buckling with couplings in vertical wells," *Cluster Computing*, vol. 22, no. S5, pp. 12283–12295, 2019.

[20] A. Y. Grigorenko, W. H. Müller, R. Wille, and I. A. Loza, "Nonaxisymmetric vibrations of radially polarized hollow cylinders made of functionally gradient piezoelectric materials," *Continuum Mechanics and Thermodynamics*, vol. 24, no. 4–6, pp. 515–524, 2012.

[21] W. G. Abdelrahman, A. Z. Al-Garni, S. I. Abdelmaksoud, and A. Abdallah, "Effect of piezoelectric patch size and material on active vibration control of wind turbine blades," *Journal of Vibration Engineering and Technonlgies*, vol. 20, no. 9, pp. 155–161, 2018.

[22] I. Lurie, *Alexander Belyaev. Theory of Elasticity*, pp. 123–125, Springer, Berlin, Germany, 2005.

[23] S. Lin, "Coupled vibration of isotropic metal hollow cylinders with large geometrical dimensions," *Journal of Sound and Vibration*, vol. 305, no. 7, pp. 308–316, 2007.

[24] R. Hill and E. H. Lee, "The theory of combined plastic and elastic deformation with particular reference to a thick tube under internal pressure," *Proceedings of the Royal Society A: Mathematical, Physical and Engineering Sciences*, vol. 191, no. 1026, pp. 278–303, 1947.

[25] L. L. Cheng, "The finite element and experimental analysis of the natural frequency of the cantilever sheet and model verification based on levy method," *Applied Mechanics and Materials*, vol. 344, pp. 132–135, 2013.

[26] M. Hussain and M. N. Naeem, "Vibration analysis of single-walled carbon nanotubes using wave propagation approach," *Mechanical Sciences*, vol. 8, no. 8, pp. 155–164, 2017.

[27] Ş. Selçuk Bayın, "Partial differential equations in cylindrcial coordinates," in *Essentials of Mathematical Methods in Science and Engineering*, pp. 237–247, John Wiley & Sons, Hoboken, NJ, USA, 2008.

[28] G. D. Pasquale and A. Soma, "Dynamic identification of electrostatically actuated MEMS in the frequency domain," *Mechanical Systems & Signal Processing*, vol. 24, no. 6, pp. 1621–1633, 2010.

[29] A. Giwa, "Solving the dynamic models of reactive packed distillation process using difference formula approaches," *Journal of Engineering & Applied Sciences*, vol. 9, no. 2, pp. 98–108, 2014.

[30] A. D. Pietro, J. P. Fernández-García, F. Ferrera et al., "Experimental investigation of exotic clustering in 13 B and 14 C using the resonance scattering method," *Journal of Physics Conference Series*, vol. 966, no. 1, Article ID 012040, 2018.

[31] M. Hussain, M. N. Naeem, A. Shahzad, and M. He, "Vibrational behavior of single-walled carbon nanotubes based on cylindrical shell model using wave propagation approach," *AIP Advances*, vol. 7, no. 4, pp. 1–16, 2017.

[32] M. Hussain and M. N. Naeem, "Vibrational behavior of single-walled carbon nanotubes based on donnell shell theory using wave propagation approach," in *Novel Nanomaterials—Synthesis and Applications*, pp. 78–90, IntechOpen, London, UK, 2018.